DOI: 10.1002/ejic.200700129

Synthesis, Structure and Magnetic Behaviour of Manganese(II) Selenolate Complexes $^1_\infty$[Mn(SePh)$_2$], [Mn(SePh)$_2$(bipy)$_2$] and [Mn(SePh)$_2$(phen)$_2$] (bipy = bipyridyl, phen = phenanthroline)

Andreas Eichhöfer,*[a] Paul T. Wood,[b] Raghavan Viswanath,[a] and Richard A. Mole[c]

Keywords: Transition-metal complexes / Manganese / X-ray structure analysis / Magnetism

The manganese selenolate complex $^1_\infty$[Mn(SePh)$_2$] has been prepared by reaction of Mn(OOCCH$_3$)$_2$ with 2 equiv. PhSeSiMe$_3$ in thf. In the crystal structure, the compound forms one-dimensional chains, and the bridging selenolate ligands result in relatively short metal–metal contacts of about 3 Å. Reaction with two equivalents of the Lewis bases 2,2′-bipyridine and 1,10-phenanthroline yielded the monomeric octahedral complexes [Mn(SePh)$_2$(2,2′-bipy)$_2$] and [Mn(SePh)$_2$(1,10-phen)$_2$], respectively. The magnetic and optical properties of these complexes have been investigated.

Introduction

Metal chalcogenolato complexes have attracted interest because of their rich structural chemistry,[1–3] their potential use as precursors for M/Se materials[4,5] and their relevance as models for active sites of chalcogen-containing metalloproteins.[6,7] Manganese, for example, plays a role as a dopant for 12–16 semiconductor films and nanocrystals, referred to as dilute magnetic semiconductors (DMS),[8,9] as well as in some manganese–oxido cluster complexes such as [Mn$_{12}$O$_{12}$(O$_2$CCH$_3$)$_{16}$][10] and [Mn$_{84}$O$_{72}$(O$_2$CMe)$_{78}$(OMe)$_{24}$(MeOH)$_{12}$(H$_2$O)$_{42}$(OH)$_6$],[11] which are known as single-molecule magnets (SMMs). With respect to manganese chalcogenolato complexes, two synthetic approaches have been widely used. The reaction of a manganese(II) halide with NaEPh (E = S, Se, Te) in the presence of quarternary ammonium or phosphonium salts yields anionic monomeric and oligomeric complexes {for example, [Mn(EPh)$_4$]$^{2-}$ (E = S, Se, Te),[12,13] [Mn$_2$(SPh)$_6$]$^{2-}$[14] and [Mn$_4$(SPh)$_{10}$]$^{2-}$[12]}. In contrast, a few neutral complexes containing bulky organic groups, such as [Mn{N(SiMe$_3$)$_2$}-(μ-SeC$_6$H$_2$-2,4,6-*i*Pr$_3$)(THF)],[15] [Mn(SeMes*)$_2$C$_4$H$_8$O] (Mes* = C$_6$H$_2$-2,4,6-*t*Bu$_3$), [Mn(SeC$_6$H$_3$-2,6-Mes$_2$)$_2$] (Mes = C$_6$H$_2$-2,4,6-Me$_3$)[16] and $^1_\infty$[Mn(SeC$_6$H$_2$-2,4,6-CH$_3$)$_2$],[17] have been synthesised by reaction of [Mn{N(SiMe$_3$)$_2$}$_2$] with the corresponding selenol RSeH (R = organic group).

Reported here is the organometallic synthesis of three manganese selenolate complexes by reaction of manganese acetate with PhSeSiMe$_3$. Structural characterization and investigation of the magnetic and optical properties of these complexes is also presented.

[a] Institut für Nanotechnologie, Forschungszentrum Karlsruhe, Postfach 3640, 76021 Karlsruhe, Germany
Fax: +7247-82-6368
E-mail: eichhoefer@int.fzk.de
[b] University Chemical Laboratory, Lensfield Rd., Cambridge CB2 1EW, UK
[c] ZWE FRM-II, Lichtenbergstrasse 1, 85747 Garching, Germany

Results and Discussion

Synthesis and Structure

The manganese selenolate complex $^1_\infty$[Mn(SePh)$_2$] (**1**) was prepared by reaction of anhydrous Mn(OOCCH$_3$)$_2$ with 2 equiv. PhSeSiMe$_3$ in thf, as shown in Scheme 1. Reaction of **1** with 2 equiv. of the Lewis bases 2,2′-bipyridine and 1,10-phenanthroline yielded dark red crystals of the monomeric octahedral complexes [Mn(SePh)$_2$(2,2′-bipy)$_2$] (**2**) and [Mn(SePh)$_2$(1,10-phen)$_2$] (**3**), respectively.

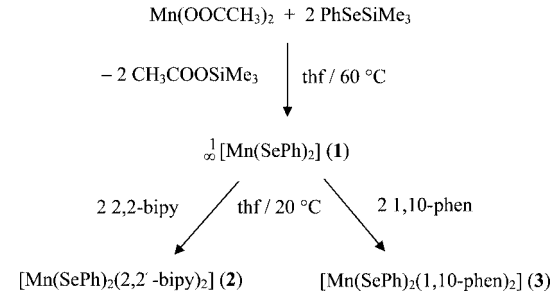

Scheme 1.

Compound **1** crystallises in the tetragonal space group $I4_1/a$. In the crystal structure of **1**, the manganese atoms are μ$_2$-bridged in one dimension by the phenylselenolato ligands to form infinite chains (Figure 1). The Mn–Se distances of 254.7(1) and 257.3(1) pm are comparable to those found in similar compounds such as [Mn(SePh)$_4$]$^{2-}$ (average 256.7 pm)[13] and $^1_\infty$[Mn(SeC$_6$H$_2$-2,4,6-CH$_3$)$_2$] (259.0 pm);[17]

the latter compound also forms a one-dimensional chain structure in the crystal lattice. However, different orientations of the phenyl rings in the structures of **1** and $^{1}_{\infty}$[Mn(SeC$_6$H$_2$-2,4,6-CH$_3$)$_2$] results in different coordination geometries around the manganese atoms. In **1**, four selenium atoms [Se(1), Se(2), Se(1′) and Se(2′)] of the phenylselenolato ligands form a distorted tetrahedral coordination environment around the manganese atom with five similar Se–Mn–Se bond angles [104.63(3)° for Se(1)–Mn(1)–Se(1′), 106.0° for Se(2′)–Mn(1)–Se(1′), 105.88(3)° for Se(1)–Mn(1)–Se(2), 107.97° for Se(2′)–Mn(1)–Se(2) and 105.42° for Se(1′)–Mn(1)–Se(2)] and only one distinctly larger angle of 125.4(1)° for Se(1)–Mn(1)–Se(2′). The Mn_2Se_2 four-membered rings in **1** have a much more rhombic–like shape [angles of 73.0(1)° for Mn(1)–Se(1)–Mn(1′) and 72.9(1)° for Mn(1)–Se(2)–Mn(1′)] than in [Mn(SeC$_6$H$_2$-2,4,6-CH$_3$)$_2$], where the manganese and selenium atoms form nearly planar quadratic rings (Mn–Se–Mn 88.0°, Se–Mn–Se 92.0°). In addition, the ring in **1** is twisted by 18.24° from ideal planarity to form a butterfly-type shape. This reduces the distance between the manganese atoms in the one dimensional chains distinctly from 359.3 pm in $^{1}_{\infty}$[Mn(SeC$_6$H$_2$-2,4,6-CH$_3$)$_2$] to 304.6 pm in **1**, which is closer to the distance between the metal atoms in [Mn(CO)$_5$]$_2$ (290.4 pm).[18]

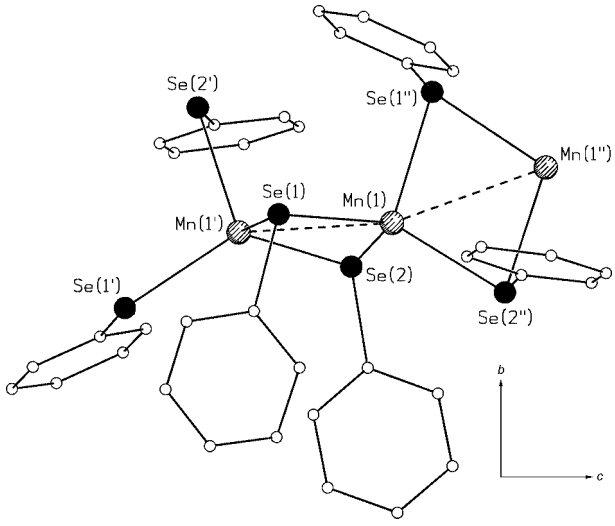

Figure 1. Section of the one-dimensional chain structure of $^{1}_{\infty}$[Mn(SePh)$_2$] (**1**) viewed down *a*. Symmetry transformation for generation of equivalent atoms: ′: *y* – 3/4, –*x* + 5/4, *z* + 1/4 ": –*y* + 5/4, *x* + 3/4, *z* – 1/4. Selected bond lengths [pm] and angles [°]: Se(1)–Mn(1) 254.7(1), Se(1)–Mn(1′) 257.3(1), Se(2)–Mn(1′) 254.8(1), Se(2)–Mn(1) 257.8(1), Mn(1)–Mn(1") 304.6(1). Mn(1)–Se(1)–Mn(1′) 73.01(3), Mn(1′)–Se(2)–Mn(1) 72.93(3), Se(1)–Mn(1)–Se(2) 105.88(3), Se(1)–Mn(1)–Se(2") 125.39(4), Se(1)–Mn(1)–Se(1") 104.63(3), Se(2′′)–Mn(1)–Se(1") 106.00(3), Se(2")–Mn(1)–Se(2) 107.97(3), Se(1")–Mn(1)–Se(2) 105.42(4), Mn(1")–Mn(1)–Mn(1′) 151.86(3).

The monomeric compound **2** crystallises in the monoclinic space group $P2_1/c$ (Figure 2) and exhibits a distorted octahedral coordination sphere around the manganese atom. The coordination sphere involves four nitrogen atoms [N(1), N(2), N(3), N(4)] from the two bidentate bipyridine ligands and two selenium atoms [Se(1), Se(2)] from the phenylselenolato ligands, which coordinate in a *cis* geometry. The Mn–Se distances are 265.3 pm and 265.5 pm, which are slightly longer than in **1**. The Mn–N distances [224.6–231.9(4) pm] as well as the N–Mn–N bite angle [N(1)–Mn(1)–N(2): 71.9(2)°, N(3)–Mn(1)–N(4): 71.5(2)°] are comparable to those in related transition-metal complexes.

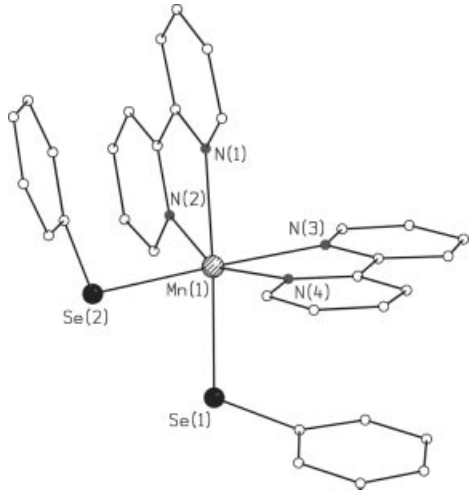

Figure 2. Molecular structure of [Mn(SePh)$_2$(2,2′-bipy)$_2$] (**2**). Selected bond lengths [pm] and angles [°]: Se(1)–Mn(1) 265.3(1), Se(2)–Mn(1) 265.5(1), Mn(1)–N(4) 224.6(4), Mn(1)–N(2) 228.3(4), Mn(1)–N(1) 228.9(4), Mn(1)–N(3) 231.9(5). N(4)–Mn(1)–N(1) 91.06(15), N(2)–Mn(1)–N(1) 71.91(16), N(4)–Mn(1)–N(3) 71.54(16), N(2)–Mn(1)–N(3) 88.81(16), N(1)–Mn(1)–N(3) 86.22(16), N(4)–Mn(1)–Se(1) 98.69(11), N(2)–Mn(1)–Se(1) 97.49(12), N(3)–Mn(1)–Se(1) 92.81(11), N(4)–Mn(1)–Se(2) 100.32(12), N(2)–Mn(1)–Se(2) 98.92(13), N(1)–Mn(1)–Se(2) 93.71(12), Se(1)–Mn(1)–Se(2) 88.74(4).

Complex **3** crystallises in the acentric space group *Cc* and is isostructural to **2**, with only slight differences in the bond lengths and bond angles.

Magnetic Properties

The magnetic behaviour of chain compounds such as **1** is well understood.[19] For materials with an antiferromagnetic exchange interaction there should be a broad maximum in the temperature dependence of the susceptibility that is typical of short-range order found in low dimensional materials. The temperature at which the maximum occurs is dependent on the size of the *intra*chain exchange coupling, *J*. For small spins, the susceptibility is normally well modelled by the approach of Bonner and Fisher,[20] which was subsequently modified by Weng.[21] For Mn^{II} chains, the larger $S = 5/2$ spin is usually better modelled[22] by the classical approach of Fisher.[23] In the case of compound **1**, the magnitude of the susceptibility is much lower than expected (the susceptibility of an array of non-interacting $S = 5/2$ ions at 300 K should be approximately 0.015 cm^3 mol^{-1}, almost an order of magnitude larger than the observed value) and it decreases smoothly down to 25 K (Figure 3). This is indica-

tive of very strong superexchange as the broad maximum must occur at a temperature far higher than 300 K. Strong exchange is expected for bridging ligands that have heavy donor atoms, although this does not seem to always be the case.[19] However, sulfur-mediated superexchange has recently been shown to give strong exchange and relatively high magnetic ordering temperatures.[24]

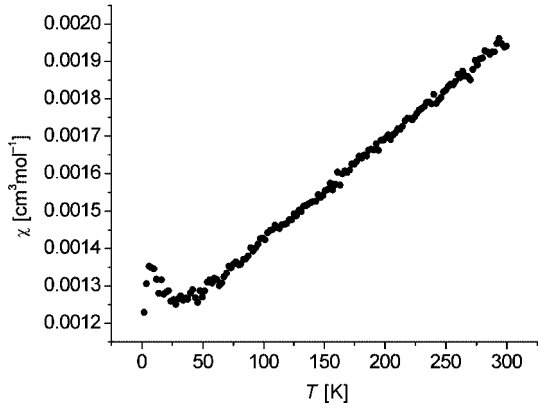

Figure 3. Susceptibility versus temperature for $^{1}_{\infty}$[Mn(SePh)$_2$] (**1**).

At the suggestion of a referee we prepared the previously reported compound $^{1}_{\infty}$[Mn(SeC$_6$H$_2$-2,4,6-CH$_3$)$_2$][17] and measured its magnetic susceptibility (Figure 4). The presence of the broad maximum centred close to 100 K shows that the exchange is strong, but not as strong as that in **1**. Fits to the Weng (Equation 1) and Fisher (Equation 2) equations give satisfactory agreement for the position of the maximum, but fail to model the low-temperature data. Fits obtained by using the Weng equation are superior to those obtained from the Fisher equation, which is surprising given the way these functions were derived (see above). These fits give values for J of –13.50(5) K and –11.2(3) K, respectively. Below 25 K there is a discontinuity in the susceptibility for both **1** and $^{1}_{\infty}$[Mn(SeC$_6$H$_2$-2,4,6-CH$_3$)$_2$], which we ascribe to the onset of long-range order.

MnSe has an analogous structure to sodium chloride and orders antiferromagnetically at 249 K,[25] which indicates that coupling is strong in this compound. In compound **1**, the Mn–Se–Mn bridging angle is approximately 73° in comparison with 90° in MnSe and 88° in $^{1}_{\infty}$[Mn(SeC$_6$H$_2$-2,4,6-CH$_3$)$_2$]. As the strength of the superexchange is dependent on the bridging angle, it is reasonable that the ordering temperatures for these three compounds should be different. Whilst there has been much study of the variation in exchange coupling with bridging angle for angles of 90° and greater, the lack of compounds with more acute bridges has meant that there has been no equivalent study for angles less than 90°. Selenolate bridges appear to favour more acute bridging angles than either alkoxide or thiolate ligands, hence further study of how the selenolate-mediated exchange interaction varies with angle would be useful. For compound **1** it is also important to remember that the Mn–Mn distance is very small, and we cannot rule out some contribution from direct exchange.

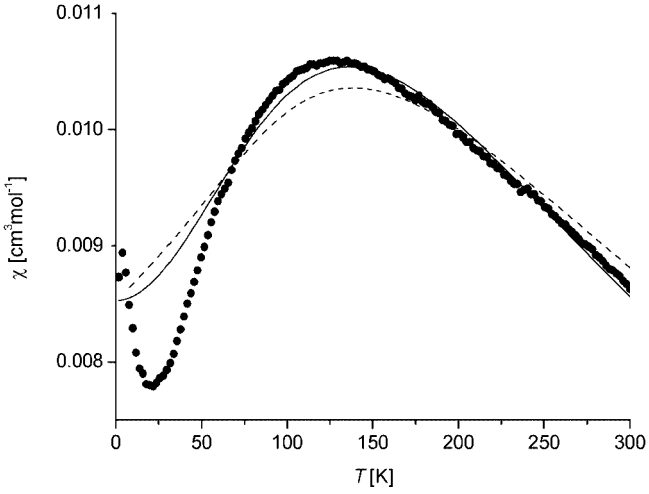

Figure 4. Susceptibility versus temperature for $^{1}_{\infty}$[Mn(SeC$_6$H$_2$-2,4,6-CH$_3$)$_2$] (dotted line). The fits according to either the Weng (straight) or Fisher (dashed) equation (see text).

For the spin Hamiltonian $\hat{H} = -2J\sum_i S_i \cdot S_{i+1}$, these equations, Equation (1) and Equation (2), have the form:

$$\chi = \frac{Ng^2\beta^2}{kT}\left(\frac{2.9167 + 208.04(J/kT)^2}{1 + 15.543(J/kT) + 2707.2(J/kT)^3}\right) \quad (1)$$

$$\chi = \frac{Ng^2\beta^2 S(S+1)}{3kT}\left(\frac{1+u}{1-u}\right)$$
$$u = \coth[2JS(S=1)/kT] - kT/[2JS(S+1)] \quad (2)$$

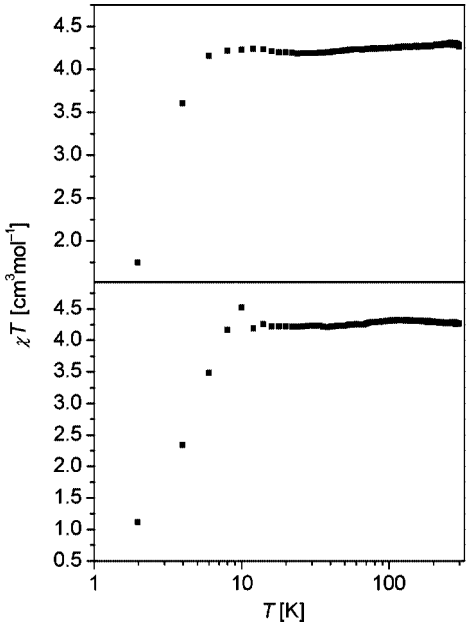

Figure 5. Graph of χT vs. T for [Mn(SePh)$_2$(2,2′-bipy)$_2$] (**2**) (bottom) and for [Mn(SePh)$_2$(1,10-phen)$_2$] (**3**) (top).

Compounds **2** and **3** are both well-isolated octahedral molecules with somewhat distorted coordination environments. They both obey the Curie law at temperatures above 10 K to give Curie constants of 4.27(8) and 4.31(1) $cm^3 mol^{-1} K$, respectively, in comparison to the expected value of 4.375 $cm^3 mol^{-1} K$ for $g = 2$ (Figure 5). Below 10 K, both compounds exhibit a local maximum in χ, followed by a sharp decrease. The single ion anisotropy of a high spin d^5 ion may be modelled according to ref.[19], however, this approach alone does not successfully model the low temperature data for either compound. We therefore suggest that the low temperature behaviour is a combination of very weak single ion anisotropy and dipolar coupling.

Optical Properties

Crystals of **1** appear red-brown in compact form but turn light rose-red when ground to a powder. The UV/Vis spectrum of **1** dissolved in thf is displayed in the lower part of Figure 6. The spectrum shows three distinct regions of absorption features, which differ significantly in their absorption intensity. The broad and intense band centred around 260 nm ($\varepsilon = 2.4 \times 10^4$ $M^{-1} cm^{-1}$), which comprises a weakly resolved shoulder, can be assigned to π–π* transitions of the phenylselenolato ligands. In the region between 340 and 400 nm, two additional weakly resolved shoulders with extinction coefficients between 200 and 400 $M^{-1} cm^{-1}$ can be thought to originate from ligand-to-metal charge transfer transitions, although they are relatively low in intensity, as well as from d–d transitions in Mn^{2+} ions. Between 400 and 700 nm one observes one sharp band at 431 nm ($\varepsilon = 12$ $M^{-1} cm^{-1}$) followed by two shoulders at 476 and 552 nm, which can be assigned because of their low intensity as d–d transitions in Mn^{2+} [$^4T_1(G) \leftarrow {}^6A_1$ 552 nm (18116 cm^{-1}), $^4T_2(G) \leftarrow {}^6A_1$ 476 nm (21008 cm^{-1}), $^4E(G) \leftarrow {}^6A_1$ 431 nm (23202 cm^{-1})].[26] The solid-state spectrum as a nujol mull (Figure 6, upper part) displays, in principle, similar absorption features as observed in solutions of **1**, although the bands differ slightly in intensity, position and shape. The strong band of the π–π* transitions of the $SePh^-$ ligands is shifted to 243 nm, and the intensity of the shoulder is reduced. Bands for the transitions at 378 and 357 nm observed in the solution spectrum are obscured by a broad band centred around 324 nm in the solid-state spectrum. A shoulder is visible at 400 nm in the solid-state spectrum, which has no equivalent in the solution spectrum. In the region of the d–d transitions, the solid-state spectrum shows a weakly resolved maximum at 436 nm, a shoulder at 464 nm and a comparatively strong band at 481 nm. The shoulder in the solution spectrum at 552 nm is only visible in the solid-state spectrum as a tail of the absorption at 481 nm. The differences observed between the solution and solid-state spectra, which are due in part to the non-validity of the Lambert–Beer law for the solid-state spectra, might also indicate different coordination geometries of the Mn^{2+} ions in thf and in the solid state. In the crystal structure of **1**, the Mn^{2+} ions are coordinated by four selenium atoms of the phenylselenolato ligands in a tetrahedrally distorted arrangement. In solution, the one-dimensional polymeric structure might be destroyed with additional coordination of thf solvent molecules, which can either result in a tetrahedral or octahedral geometry or a mixture of both.

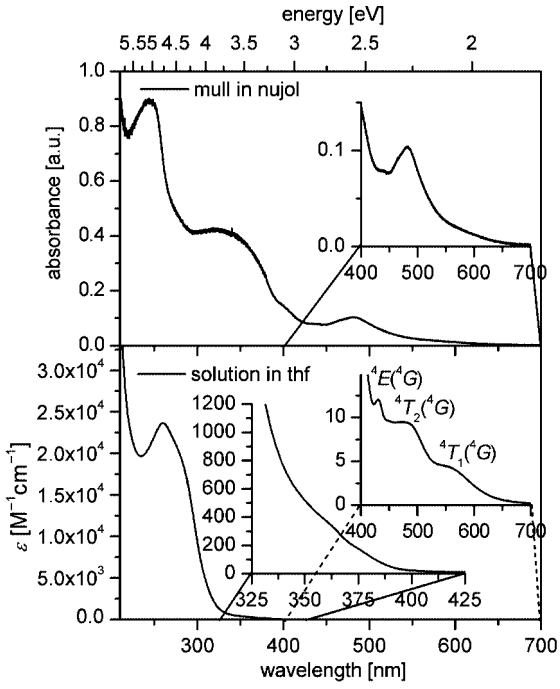

Figure 6. UV/Vis spectra of $^1_\infty$[Mn(SePh)$_2$] (**1**) in thf.

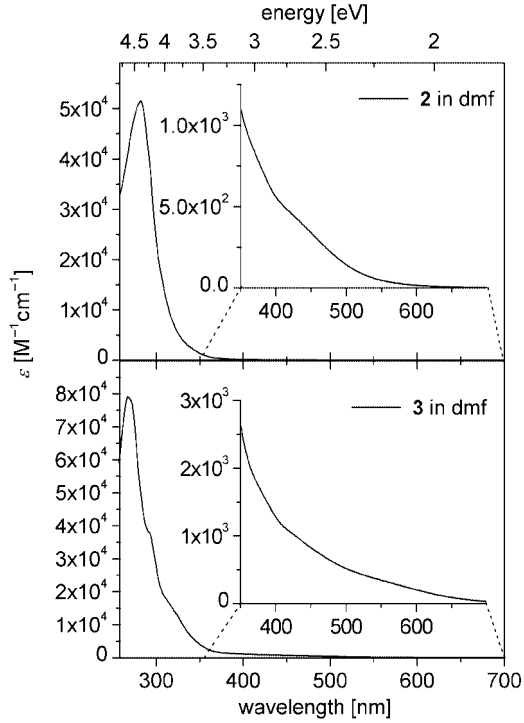

Figure 7. UV/Vis spectra of [Mn(SePh)$_2$(2,2′-bipy)$_2$] (**2**) (top) and [Mn(SePh)$_2$(1,10-phen)$_2$] (**3**) (bottom) in dmf.

The dark red crystals of **2** and **3** mostly keep their colour when ground to a powder. In dmf solutions, **2** and **3** display strong absorption features at 284 nm and 267 nm, respectively, which can be assigned to π–π* transitions of either the bidentate amine ligands or the $PhSe^-$ ligands, or a mixture of both (Figure 7). The UV/Vis spectrum of **3** displays several shoulders at 292, 313 and 322 nm. Apart from the strong absorption, weakly resolved shoulders between 350 and 600 nm (**2**), and 350 and 700 nm (**3**) could originate from metal-to-ligand charge transfer transitions into low-lying, empty π* orbitals of the bipyridyl and phenanthroline ligands, respectively. An assignment as d–d transitions seems to be unlikely because of extinction coefficients in the region between 500 and 2000 $M^{-1}cm^{-1}$. These transitions are most probably obscured by the charge-transfer bands.

Experimental Section

Synthesis: Standard Schlenk techniques were employed throughout the syntheses by using a double manifold vacuum line with high-purity dry nitrogen. The solvents thf and diethyl ether were dried with sodium benzophenone and distilled under nitrogen. Anhydrous dimethylformamide (dmf) ($H_2O < 0.005\%$) obtained from Aldrich was degassed, freshly distilled and stored over molecular sieves under nitrogen. $Mn(OOCCH_3)_2$, 2,2′-bipyridine and 1,10-phenanthroline were purchased from Aldrich. $PhSeSiMe_3$ was prepared according to a literature procedure.[27]

$^1_\infty$[Mn(SePh)$_2$] (1): An ultrasonic bath was used to suspend $Mn(OOCCH_3)_2$ (0.42 g, 2.45 mmol) in thf (45 mL) for 45 min. $PhSeSiMe_3$ (0.98 mL, 5.1 mmol) was then added, and the mixture was stirred overnight to give an orange solution. Careful addition of diethyl ether (50 mL) resulted in the crystallisation of dark red needles of $^1_\infty$[Mn(SePh)$_2$] (**1**). Filtration of the crude product, and further addition of diethyl ether to the filtrate resulted in a total yield of 90% (0.81 g) of **1**. $C_{12}H_{10}MnSe_2$ (367.1): calcd. C 39.3, H 2.8; found C 39.8, H 3.1.

[Mn(SePh)$_2$(2,2′-bipy)$_2$] (2): $^1_\infty$[Mn(SePh)$_2$] (0.15 g, 0.41 mmol) was dissolved in thf (25 mL) to give an orange-brown solution. A solution of 2,2′-bipyridine (0.13 g, 0.83 mmol) in thf (6 mL) was then added, and the mixture immediately turned dark red. Overnight, a dark red crystalline precipitate of [Mn(SePh)$_2$(2,2′-bipy)$_2$] (**2**) was formed from this solution with a total yield of 79% (0.22 g). Compound **2** was insoluble in thf and could be recrystallised for purification from dmf/thf. $C_{32}H_{26}MnN_4Se_2$ (679.4): calcd. C 56.6, H 3.7, N 8.3; found C 56.4, H 4.1, N 8.1. Crystals suitable for single-crystal X-ray analysis were grown by layering dmf solutions of **2** with diethyl ether.

[Mn(SePh)$_2$(1,10-phen)$_2$] (3): $^1_\infty$[Mn(SePh)$_2$] (0.081 g, 0.22 mmol) was dissolved in thf (20 mL) to give an orange-brown solution. A solution of 1,10-phenanthroline (0.083 g, 0.46 mmol) in thf (5 mL) was then added, which led to the immediate formation of [Mn(SePh)$_2$(1,10-phen)$_2$] (**3**) as a cherry red crystalline precipitate with a total yield of 84% (0.15 g). $C_{36}H_{26}MnN_4Se_2{\cdot}C_3H_7NO$ (800.6): calcd. C 58.6, H 4.2, N 8.8; found C 58.7, H 4.2, N 8.7. Crystals suitable for single-crystal X-ray analysis were grown by layering dmf solutions of **3** with diethyl ether.

Crystallography: Crystals suitable for single-crystal X-ray diffraction were taken directly from the reaction solution of the compound and then selected under perfluoroalkylether oil. Single-crystal X-ray diffraction data of compounds **1**–**3** were collected by using graphite-monochromatised Mo-K_α radiation (λ = 0.71073 Å) on a STOE IPDS II (Imaging Plate Diffraction System) equipped with a Schneider rotating anode. Raw intensity data were collected and treated with the STOE X-Area software Version 1.27. Data for all compounds were corrected for Lorentz and polarisation effects. The structures were solved with the direct methods program SHELXS[28] of the SHELXTL PC suite programs and were refined with the use of the full-matrix least-squares program SHELXL.[28] Molecular diagrams were prepared with SCHAKAL 97.[29]

All Mn, Se, N and C atoms, with the exception of the C atoms of thf in **1**, were refined with anisotropic displacement parameters, whilst H atoms were calculated in fixed positions (Table 1).

Table 1. Crystallographic data for $^1_\infty$[Mn(SePh)$_2$] (**1**), [Mn(SePh)$_2$(2,2′-bipy)$_2$] (**2**) and [Mn(SePh)$_2$(1,10-phen)$_2$] (**3**).

	1·0.4thf	**2**	**3**·dmf
F_w [g mol^{-1}]	395.9	679.4	800.6
Crystal system	tetragonal	monoclinic	monoclinic
Space group	$I4_1/a$	$P2_1/c$	Cc
a [Å]	22.051(3)	10.238(2)	15.406(3)
b [Å]		17.444(4)	16.747(3)
c [Å]	11.443(2)	16.651(3)	13.578(3)
β [°]		102.99(3)	101.74(3)
V [Å^3]	5563.8(16)	2897.7(10)	3430.1(12)
Z	16	4	4
T [K]	190	180	190
d_c [g cm^{-3}]	1.891	1.557	1.550
μ(Mo-K_α) [mm^{-1}]	6.159	2.996	2.547
F[000]	3056	1356	1612
$2\theta_{max}$ [°]	52	49	49
Measured reflections	4236	16985	10401
Unique reflections	2372	4616	5163
R_{int}	0.0446	0.0666	0.1128
Reflections with $I > 2\sigma(I)$	1746	3306	4441
Parameters	139	352	429
$R_1[I > 2\sigma(I)]$[a]	0.0459	0.0498	0.0667
wR_2(all data)[b]	0.1295	0.1292	0.1892
Abs. struct. param.			0.27(2)

[a] $R_1 = \Sigma||F_o| - |F_c||/\Sigma|F_o|$. [b] $wR_2 = \{\Sigma[w(F_o^2 - F_c^2)^2] / \Sigma[w(F_o^2)^2]\}^{1/2}$.

CCDC-603930(**1**), -603931(**2**) and -603932(**3**) contain the supplementary crystallographic data for this paper. These data can be obtained free of charge from The Cambridge Crystallographic Data Centre via www.ccdc.cam.ac.uk/data_request/cif.

Physical Measurements: Field-cooled SQUID measurements were performed at 1 T with an extraction magnetometer (Quantum Design PPMS) in DC extraction mode, and the response to the vertical movement of the sample (10 ms^{-1}) through the detection coils was recorded, under a dry helium environment. The samples were contained in high-precision quartz glass sample holders owing to the high degree of moisture sensitivity of the compounds. The data were corrected for the sample holder and for diamagnetism using Pascal's constants.[19] UV/Vis absorption spectra of cluster molecules in solution were measured on a Varian Cary 500 spectrophotometer in quartz cuvettes. Solid-state reflection spectra were measured as micron-sized crystalline powders between quartz plates with a Labsphere integrating sphere.

Acknowledgments

This work was supported by the Deutsch-Israelisches Programm (DIP) and the Deutsche Forschungsgemeinschaft (center for func-

tional nanostructures CFN). The authors are grateful to Prof. Dr. D. Fenske for helpful discussions and generous support and to E. Tröster for her assistance in the practical work.

[1] I. Dance, K. Fisher, *Prog. Inorg. Chem.* **1994**, *41*, 637–803.
[2] S. Dehnen, A. Eichhöfer, D. Fenske, *Eur. J. Inorg. Chem.* **2002**, 279–317.
[3] M. W. DeGroot, J. F. Corrigan, *Comprehensive Coordination Chemistry II* (Eds.: M. Fujita, A. Powell, C. Creutz), Pergamon, Oxford, **2004**, Vol. 7, pp. 57–123.
[4] J. Arnold, *Prog. Inorg. Chem.* **1995**, *43*, 353.
[5] M. Bochmann, *Chem. Vap. Deposition* **1996**, *2*, 85–96.
[6] B. Krebs, G. Henkel, *Angew. Chem.* **1991**, *103*, 785–804; *Angew. Chem. Int. Ed. Engl.* **1991**, *30*, 769–788.
[7] B. Krebs, G. Henkel, *Chem. Rev.* **2004**, *104*, 801–824.
[8] J. K. Furdyna, *J. Appl. Phys.* **1988**, *64*, R29–R64.
[9] D. J. Norris, N. Yao, F. T. Charnock, T. A. Kennedy, *Nanoletters* **2001**, *1*, 3–7.
[10] R. Sessoli, H.-K. Tsai, A. R. Schake, S. Wang, J. B. Vincent, K. Folting, D. Gatteschi, G. Cristou, D. N. Hendrickson, *J. Am. Chem. Soc.* **1993**, *115*, 1804–1816.
[11] A. J. Tasiopoulous, A. Vinslava, W. Wernsdorfer, K. A. Abboud, G. Christou, *Angew. Chem. Int. Ed.* **2004**, *43*, 2117–2121.
[12] T. Costa, J. Dorfman, K. S. Hagen, R. H. Holm, *Inorg. Chem.* **1983**, *22*, 4091–4099.
[13] W. Tremel, B. Krebs, K. Greiwe, W. Simon, H. Stephan, G. Henkel, *Z. Naturforsch., Teil B* **1992**, *47*, 1580–1592.
[14] H. Stephan, K. Griesar, W. Haase, G. Henkel, *Z. Naturforsch.* **1994**, *49b*, 1620–1632.
[15] M. Bochmann, A. K. Powell, X. Song, *Inorg. Chem.* **1994**, *33*, 400–401.
[16] J. J. Ellison, K. Ruhlandt-Senge, H. H. Hope, P. P. Power, *Inorg. Chem.* **1995**, *34*, 49–54.
[17] M. Bochmann, A. K. Powell, X. Song, *J. Chem. Soc. Dalton Trans.* **1995**, 1645–1648.
[18] R. Bianchi, G. Gervasio, D. Marabello, *Inorg. Chem.* **2000**, *39*, 2360–2366.
[19] O. Kahn, *Molecular Magnetism*, Wiley-VCH, Weinheim, **1993**.
[20] J. C. Bonner, M. E. Fisher, *Phys. Rev. A* **1964**, *135*, A640.
[21] C. Y. Weng, Ph. D. Thesis, Carnegie Mellon University, Pittsburgh PA, USA, **1969**.
[22] S. O. H. Gutschke, D. J. Price, A. K. Powell, P. T. Wood, *Inorg. Chem.* **2000**, *39*, 3705.
[23] M. E. Fisher, *Am. J. Phys.* **1964**, *32*, 343.
[24] S. M. Humphrey, A. Alberola, C. J. Gomez Garcia, P. T. Wood, *Chem. Commun.* **2006**, 1607.
[25] T. Ito, K. Ito, M. Oka, *Jpn. J. Appl. Phys.* **1978**, *17*, 371.
[26] A. B. P. Lever, *Inorganic Electronic Spectroscopy*, 2nd ed., Elsevier, Amsterdam, **1984**, p. 448.
[27] N. Miyoshi, H. Ishii, K. Kondo, S. Mui, N. Sonoda, *Synthesis* **1979**, 301–304.
[28] G. M. Sheldrick, *SHELXTL PC version 5.1 An Integrated System for Solving, Refining, and Displaying Crystal Structures from Diffraction Data*, Bruker Analytical X-ray Systems, Karlsruhe, **2000**.
[29] E. Keller, *SCHAKAL 97*, *A Computer Program for the Graphic Representation of Molecular and Crystallographic Models*, University of Freiburg, **1997**.

Received: January 30, 2007
Published Online: September 4, 2007

